

# HQ-DM: Single Hadamard Transformation-Based Quantization-Aware Training for Low-Bit Diffusion Models

Shizhuo Mao\* Hongtao Zou\* Qihu Xie Song Chen Yi Kang†

University of Science and Technology of China

Hefei, China

{msz123, zouht49, xieqihu}@mail.ustc.edu.cn, {songch, ykang}@ustc.edu.cn

## Abstract

*Diffusion models have demonstrated significant applications in the field of image generation. However, their high computational and memory costs pose challenges for deployment. Model quantization has emerged as a promising solution to reduce storage overhead and accelerate inference. Nevertheless, existing quantization methods for diffusion models struggle to mitigate outliers in activation matrices during inference, leading to substantial performance degradation under low-bit quantization scenarios. To address this, we propose **HQ-DM**, a novel Quantization-Aware Training framework that applies Single Hadamard Transformation to activation matrices. This approach effectively reduces activation outliers while preserving model performance under quantization. Compared to traditional Double Hadamard Transformation, our proposed scheme offers distinct advantages by seamlessly supporting INT convolution operations while preventing the amplification of weight outliers. For conditional generation on the ImageNet 256×256 dataset using the LDM-4 model, our W4A4 and W4A3 quantization schemes improve the Inception Score by 12.8% and 467.73%, respectively, over the existing state-of-the-art method.*

## 1. Introduction

In recent years, deep generative models have exhibited remarkable capabilities across multiple modalities, including image [25, 39, 41], speech [32, 33, 53], and text [7, 11, 52]. Among them, diffusion models [21, 41, 62, 67], known for their superior generative quality and stable training dynamics, have emerged as a new mainstream generative framework following Generative Adversarial Networks (GANs) [17] and autoregressive models [53–55]. They have achieved notable breakthroughs in tasks such as

high-resolution image synthesis [31, 44, 58], image editing [3, 6, 35], and video generation [5, 22, 49].

However, the impressive performance of diffusion models incurs substantial computational overhead. Their generation process relies on a multi-step denoising sampling procedure [21], resulting in prolonged inference latency and high memory consumption, which hinder their applicability in real-time or resource-constrained scenarios. Recent studies [34, 51] have sought to reduce the number of denoising iterations during the diffusion process to alleviate overall inference latency. Although these methods partially improve generation efficiency, the noise prediction network remains heavily parameterized, leading to considerable computational complexity and memory overhead, and thus failing to fundamentally overcome the performance bottlenecks of deploying diffusion models on resource-limited devices.

To mitigate these computational challenges, researchers have introduced a range of model compression and acceleration techniques, including pruning [1, 14, 29], distillation [45, 47, 64], low-rank decomposition [8, 69], and quantization [16, 30, 42, 47, 64]. Among them, quantization has emerged as a research focus in recent years, as it can substantially reduce computational and storage overhead while maintaining nearly the same model performance. Existing quantization approaches are typically categorized into two types: Post-Training Quantization (PTQ) and Quantization-Aware Training (QAT). PTQ [36] performs offline discretization of weights and activations after training, offering ease of deployment and low implementation cost, but it may suffer from notable accuracy degradation in complex generative tasks. In contrast, QAT [12, 27] introduces quantization noise during training, enabling the model to adapt to low-precision arithmetic through gradient-based optimization, thereby achieving a more favorable balance between model accuracy and quantization efficiency.

Nevertheless, applying quantization techniques directly to diffusion models presents significant and unique challenges. Unlike traditional classification or generative tasks, the activations of the noise prediction network in diffusion

\*These authors contributed equally.

†Corresponding authors.

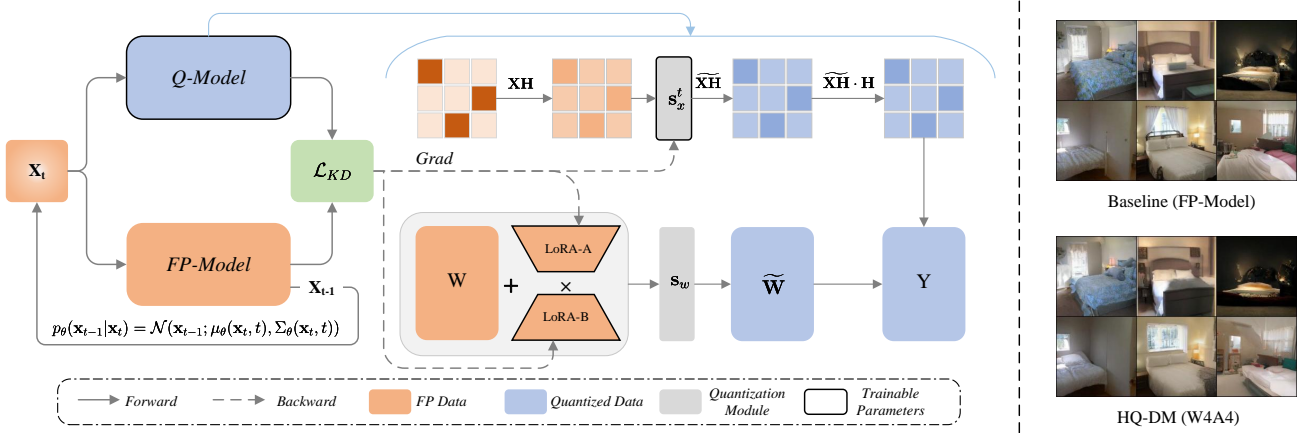


Figure 1. Overview diagram of the HQ-DM distillation framework, illustrating the application of Single Hadamard transformation before activation quantization to reduce outliers, followed by hardware-efficient implementation of matrix multiplication and convolution operations using quantized integer matrices.

models exhibit strong non-stationarity during the multi-step denoising process: the scale of input noise, feature structures, and statistical properties vary substantially across timesteps, leading to continuously shifting activation distributions throughout sampling [30, 38]. Moreover, the prevalent long-tailed and outlier characteristics in diffusion models further enlarge the activation dynamic range, making them susceptible to significant clipping and rounding errors under low-bit quantization. More critically, these errors accumulate over multiple denoising steps, resulting in cumulative and amplified degradation of generation quality. Consequently, the non-stationary and outlier behaviors of activations constitute the key bottlenecks that hinder accurate quantization of diffusion models, calling for systematic solutions to mitigate their impact.

Several recent studies have begun to explore the challenges of temporal quantization in diffusion models. For instance, Li et al. [30] identified the issues of temporal variation in activation distributions and the accumulation of quantization errors, and proposed a timestep-aware calibration mechanism to mitigate performance degradation in PTQ. Similarly, So et al. [50] further analyzed how temporal activation dynamics influence quantization interval selection. Although these works highlight the temporal non-stationarity of diffusion models, most remain confined to the Post-Training Quantization (PTQ) framework and do not systematically address the problem from the perspectives of outlier dispersion in the transform domain and training-phase quantization optimization (e.g., QAT).

QuaRot introduces the Hadamard transformation into PTQ for LLMs, yet it fails to adequately adjust quantization factors after incorporating the Hadamard transformation. Xi et al. [60] incorporate the Hadamard transfor-

ation into quantization-aware training but do not account for the optimization of time-step-dependent quantization factors. Moreover, due to its adoption of the Double Hadamard Transformation, it lacks support for integer convolution computation modules, and the offline-generated Hadamard-transformed weight matrices amplify quantization errors.

To tackle these challenges, this paper introduces a Single Hadamard Transformation-Based Quantization-Aware Training (QAT) method for diffusion models, which mitigates outlier effects via the Hadamard transformation and integrates LoRA-based weight fine-tuning with timestep-wise learnable quantization factors. This design significantly alleviates the accumulation of quantization errors under data-free fine-tuning conditions. Experimental results show that our method substantially improves generation quality at the W4A4 / W4A3 quantization level, demonstrating its practicality and strong generalization potential for diffusion model quantization.

Overall, the main contributions of this paper are summarized as follows:

(1) We pioneer a Single Hadamard Transformation-based distillation framework that reduces activation outliers prior to quantization through Hadamard transformation, thereby enhancing diffusion model performance under low-bit quantization settings.

(2) We propose, for the first time, the Single Hadamard Transformation, which is hardware-efficient. This transformation addresses two critical limitations of the conventional Hadamard transform: its inability to support INT convolution operations and its tendency to generate additional outliers in weight matrices during computation.

(3) HQ-DM demonstrates exceptional performance across multiple datasets and models, surpassing existing

SOTA methods, particularly in low-bit activation quantization scenarios. Under W4A3 quantization with the LDM-4 model on ImageNet 256×256, HQ-DM achieves a 467.73% improvement on IS score, while under W4A4 quantization it delivers a 12.8% enhancement on IS score compared to EfficientDM.

## 2. Related Work

**Quantization of Diffusion Models.** Diffusion models represent a class of generative models that learn data distributions through a progressive denoising process, typically formulated as a Markov chain that gradually transforms random noise into structured samples. Recently, quantization has been extended to diffusion models to reduce their prohibitive computational and memory overhead. Early PTQ-based approaches such as PTQ4DM [48] and Q-Diffusion [30] leverage data-free calibration by extracting intermediate activations from the denoising process. More advanced methods, including PTQ-D [18], TFMQ-DM [24], APQ-DM [56], and QuEST [57], enhance quantization precision through improved calibration and temporal feature modeling. However, PTQ-based strategies still exhibit severe performance drops at 4-bit or lower precision due to activation outliers and the non-stationary feature dynamics across timesteps. To address this issue, QAT-based methods like EfficientDM [19] incorporate fine-tuning to recover generation quality under low-bit settings. Despite the advancements achieved by these works in diffusion model quantization, these quantization schemes lead to severe performance degradation under lower-bit quantization scenarios.

**Activation Outliers and Smoothing Techniques for Model Quantization.** Post-training quantization (PTQ) is an effective approach to reduce model size and inference cost without retraining. However, neural activations often follow heavy-tailed distributions, where a few large-magnitude outliers dominate the tensor range and severely degrade quantization accuracy [4]. Early works mitigate this by clipping or architectural transformations such as Outlier Channel Splitting (OCS) [68], while recent methods for large models introduce algebraically equivalent scaling to smooth activation distributions without retraining. Notably, SmoothQuant [61] migrates quantization difficulty from activations to weights via scaling, and Outlier Suppression+ [59] refines this with channel-wise affine transformations, both proving that explicit outlier handling is key to achieve low-bit quantization. Diffusion models exhibit more complex outlier behaviors: activation statistics vary significantly across timesteps, and quantization errors can accumulate during iterative denoising. To address this, diffusion-specific PTQ methods introduce timestep- or layer-aware smoothing mechanisms. DMQ [28] analyzes outlier sources in diffusion networks and applies

diffusion-aware transformations to suppress extreme activations, while MPQ-DM [15] leverages mixed-precision allocation guided by outlier statistics to maintain quality under ultra-low-bit settings. Overall, these studies demonstrate that timestep-adaptive outlier smoothing—through equivalent scaling or precision allocation—is essential for stable and accurate quantization of diffusion models.

QuaRot [2] introduces Hadamard transformation into Post-Training Quantization (PTQ) for large language models to mitigate outliers and enhance model performance under low-bit quantization. Similarly, Xi et al. [60] incorporates the Hadamard transformation into the training framework of large models to reduce outliers and improve performance. However, these works do not optimize timestep-dependent quantization factors as training objectives. Moreover, the proposed Double Hadamard Transformation suffers from two critical limitations: incompatibility with integer-based convolution operations and the introduction of additional outliers in weight matrices, thereby hindering its effective application in diffusion models.

## 3. Background

**Diffusion Model** Diffusion Models (DMs) have emerged as one of the most powerful generative model families [21, 38, 41], achieving remarkable success in high-fidelity image synthesis [31, 44, 58], text-to-image generation [40, 43], and video generation [5, 22, 49]. These models learn to reverse a gradual noising process, transforming a simple Gaussian prior into complex data distributions through iterative denoising. Formally, the forward diffusion process progressively adds Gaussian noise to a clean data sample  $x_0$  over  $T$  timesteps:

$$q(x_t | x_{t-1}) = \mathcal{N}(x_t; \sqrt{1 - \beta_t} x_{t-1}, \beta_t I) \quad (1)$$

where  $\beta_t$  controls the noise variance at each timestep. During training, a denoising network  $\epsilon_\theta(x_t, t)$  is optimized to predict the added noise by minimizing the simplified objective:

$$\mathcal{L}_{\text{simple}} = \mathbb{E}_{x_0, t, \epsilon} [\|\epsilon - \epsilon_\theta(\sqrt{\bar{\alpha}_t} x_0 + \sqrt{1 - \bar{\alpha}_t} \epsilon, t)\|^2] \quad (2)$$

where  $\bar{\alpha}_t = \prod_{i=1}^t (1 - \beta_i)$ . To accelerate sampling, several variants have been proposed. DDIM [51] introduces deterministic sampling to reduce inference steps, while Latent Diffusion Models (LDMs) [41] perform diffusion in a compressed latent space, greatly improving efficiency.

**Model Quantization** Quantization refers to the process of mapping high-precision numbers to low-bit representations. Our research primarily focuses on the quantization from floating-point numbers to integers, which can achieve memory compression and inference acceleration. A typical quantization method is linear mapping quantization,

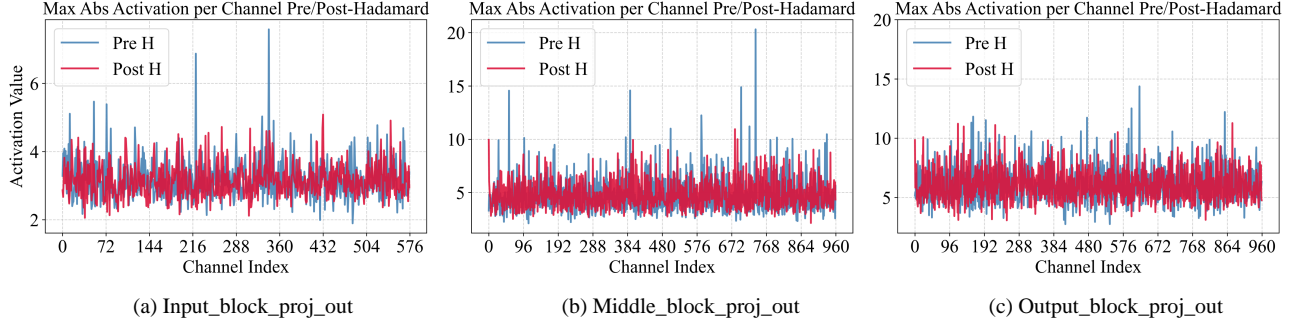


Figure 2. Channel-wise analysis of outlier distribution in activations from the input\_block, middle\_block and output\_block layer at timestep0, comparing before and after Hadamard Transformation states. Given that the minimum value of each channel in the matrix is zero, the maximum value of each channel can be considered as the outlier for that channel.

which maintains a stable quantization step size and uniformly maps values within the dynamic range to integer numbers. The formula for symmetric quantization from floating-point numbers to N-bit integers is as follows:

$$\mathbf{X}_{\text{int}} = \text{clamp} \left( \left\lfloor \frac{\mathbf{X}_{\text{fp}}}{S} \right\rfloor, \min, \max \right) \quad (3)$$

$$\hat{\mathbf{X}} = \mathbf{S} \cdot \mathbf{X}_{\text{int}} \quad (4)$$

Where  $\lfloor \cdot \rfloor$  represents the rounding function, and clamp denotes truncation within the integer range representable by N-bit precision.  $S$  represents the quantization scale factor, which is a trainable parameter in this paper. Asymmetric quantization involves adding an offset (zero-point) after dividing  $X$  by the scale factor  $S$ , which alters the dynamic range of the value distribution. Under optimal conditions, this approach effectively provides one additional bit compared to symmetric quantization, yet it faces challenges in achieving efficient INT hardware acceleration. To overcome the non-differentiability of the rounding and truncation functions during the QAT process, we adopt the Straight-Through Estimator (STE) convention:

$$\frac{\partial \text{Round}(x)}{\partial x} = 1, \quad \frac{\partial \text{Clamp}(x)}{\partial x} = \mathbb{I}_{[\min, \max]}(x) \quad (5)$$

Outliers hold significant implications in model quantization, referring to large values that substantially exceed the magnitude of other values. Due to the presence of these outliers, it becomes challenging to simultaneously preserve information from both normal values and outliers after quantization, consequently leading to substantial performance degradation in low-bit quantization scenarios. Compared to weight values, activations typically exhibit more frequent occurrences of outliers [10, 63, 66]. Therefore, to maintain model performance under low-bit quantization, it is crucial to mitigate the impact caused by these outlier values.

**Hadamard Transformation** An orthogonal matrix is defined as a real square matrix  $\mathbf{Q}$  satisfying  $\mathbf{Q}\mathbf{Q}^T = \mathbf{I}$ . The linear transformation corresponding to an orthogonal matrix preserves both vector lengths and angles between vectors, making it particularly suitable for performing linear transformations on matrices. A Hadamard matrix represents a special class of orthogonal matrices, satisfying the following recurrence relation:

$$\mathbf{H}_0 = [1] \quad (6)$$

$$\mathbf{H}_k = \frac{1}{\sqrt{2}} \begin{bmatrix} \mathbf{H}_{k-1} & \mathbf{H}_{k-1} \\ \mathbf{H}_{k-1} & -\mathbf{H}_{k-1} \end{bmatrix} \quad (7)$$

The matrix  $\mathbf{H}_k$  is of size  $2^k \times 2^k$  and possesses both orthogonality and rotational symmetry. Consequently, it satisfies

$$\mathbf{H}_k \mathbf{H}_k^\top = \mathbf{I} \quad \text{and} \quad \mathbf{H}_k = \mathbf{H}_k^\top \quad (8)$$

It can be observed that the orthonormal Hadamard matrix is defined as

$$\mathbf{H}_k = 2^{-k/2} \cdot \mathbf{H}_k^{\text{raw}} \quad (9)$$

where  $\mathbf{H}_k^{\text{raw}}$  is the unnormalized Hadamard matrix with all entries in  $\{+1, -1\}$ . This decomposition is crucial for integer-only quantized inference, ensuring that the matrix multiplication after transformation can be performed entirely within integer arithmetic. For any matrix-vector multiplication of the form  $\mathbf{H}_k \mathbf{x}$ , the computational complexity is  $\mathcal{O}(k \cdot 2^k)$  operations. The Hadamard transformation is a linear transformation that uses a Hadamard matrix as its transform kernel. Since not all dimensions are powers of two, we employ a block-diagonal Hadamard transformation:

$$\mathbf{H} = \text{BlockDiag}(\mathbf{H}_k, \mathbf{H}_k, \dots, \mathbf{H}_k), \quad (10)$$

whose dimension is a multiple of a power of two. The order  $k$  of the base Hadamard matrix  $\mathbf{H}_k$  is directly related to its

outlier-diffusion capability: larger  $k$  leads to stronger diffusion of dominant outliers across all coordinates. Fundamentally, the Hadamard transformation maps input vectors into a linear subspace with fewer extreme values, thereby significantly improving model performance under low-bit quantization.

## 4. Method

In the context of low-bit quantization for diffusion models, we employ the Hadamard transformation to suppress outliers and thereby enhance model performance under aggressive quantization. In this section, we present our Hadamard-based LoRA fine-tuning framework—termed **HQ-DM** (Single Hadamard Transformation-Based Quantization Aware Training on Diffusion Models)—which applies quantization to both activations and weights, as illustrated in Figure 1.

### 4.1. LoRA-based Distillation

Inspired by EfficientDM [19], we retain the LoRA-based distillation framework. The core idea of Low-Rank Adaptation (LoRA) is to freeze the original pre-trained weight matrix and only train a pair of low-rank update matrices that are adapted to it. This strategy drastically reduces the number of trainable parameters while preserving a sufficiently expressive parameter space, as the adaptation is concentrated on the dominant principal components of the weight updates.

Formally, consider a linear transformation  $\mathbf{Y} = \mathbf{X} \cdot \mathbf{W}$ , where  $\mathbf{X} \in \mathbb{R}^{T \times C_i}$  and  $\mathbf{W} \in \mathbb{R}^{C_i \times C_o}$ . Under LoRA, the adapted weight matrix becomes

$$\mathbf{W}' = \mathbf{W} + \mathbf{B} \cdot \mathbf{A} \quad (11)$$

where  $\mathbf{B} \in \mathbb{R}^{C_i \times r}$  and  $\mathbf{A} \in \mathbb{R}^{r \times C_o}$  are trainable low-rank matrices with  $r \ll \min(C_i, C_o)$ . In the distillation process, at denoising timestep  $t$ , the same noisy input  $\mathbf{x}_t$  is fed into both the full-precision (FP) teacher model and the quantized student model, and the mean squared error (MSE) between their outputs is minimized:

$$\mathcal{L}_{\text{distill}} = \mathbb{E}_{\mathbf{x}_t, t} \left[ \|\epsilon_{\text{FP}}(\mathbf{x}_t, t) - \epsilon_{\text{quant}}(\mathbf{x}_t, t)\|_2^2 \right] \quad (12)$$

Prior work has shown that in diffusion models, the activation distributions vary significantly across timesteps. To address this, LSQ [13] introduces timestep-aware quantization scales and optimizes them independently for each denoising step. We adopt this strategy unchanged for both weight and activation quantization in our framework.

### 4.2. Hadamard Transformation to smooth outliers

We utilize Single Hadamard Transformation to reduce outliers in the activations, while avoiding the introduction of

additional outliers in the weights that typically arises from the conventional Double Hadamard Transformation. As shown in Figure 2, the outliers in the activation values are significantly reduced after the transformation.

**Matrix Multiplication** The Hadamard transformation is applied to a 2D input matrix by multiplying the matrix to be quantized with a Hadamard matrix. Since the input channel dimension  $C_i$  is not necessarily a power of two, we construct a block-diagonal Hadamard matrix  $\mathbf{H} \in \mathbb{R}^{C_i \times C_i}$  composed of  $m$  identical submatrices  $\mathbf{H}_k$ , i.e.,

$$\mathbf{H} = \text{BlockDiag}(\underbrace{\mathbf{H}_k, \mathbf{H}_k, \dots, \mathbf{H}_k}_{m \text{ blocks}}),$$

where  $C_i = m \cdot 2^k$ . This block-diagonal structure preserves orthogonality, satisfying  $\mathbf{H}\mathbf{H}^\top = \mathbf{H}^2 = \mathbf{I}$ . In cases where the number of input channels is smaller than the base order  $k$  (e.g., during the initial projection of image features), we set  $\mathbf{H} = \mathbf{I}$ , effectively bypassing the transformation.

Given the orthogonality of the Hadamard matrix ( $\mathbf{H}^\top = \mathbf{H}^{-1} = \mathbf{H}$ ), the original activation matrix  $\mathbf{X}$  can be exactly recovered from its transformed and quantized form via inverse transformation followed by dequantization. Specifically, let  $(\mathbf{X}\mathbf{H})_{\text{int}}$  denote the integer-valued quantized representation of the transformed activations  $\mathbf{X}\mathbf{H}$ , and let  $\mathbf{S}_{\mathbf{XH}}$  be the corresponding floating-point quantization scale. Then the dequantized output is:

$$\hat{\mathbf{X}} = \mathbf{S}_{\mathbf{XH}} \cdot (\mathbf{X}\mathbf{H})_{\text{int}} \cdot \mathbf{H} \quad (13)$$

Consequently, for a linear layer  $\mathbf{Y} = \mathbf{X}\mathbf{W}$ , we insert the identity  $\mathbf{H}\mathbf{H}^\top = \mathbf{I}$  to obtain:

$$\mathbf{Y} = \mathbf{X}\mathbf{H} \cdot \mathbf{H}^\top \mathbf{W} = (\mathbf{X}\mathbf{H}) \cdot \mathbf{H} \cdot \mathbf{W} \quad (14)$$

$$\mathbf{Y} \approx \mathbf{S}_{\mathbf{XH}} \mathbf{S}_{\mathbf{W}} \cdot ((\mathbf{X}\mathbf{H})_{\text{int}} \cdot \mathbf{H} \cdot \mathbf{W}_{\text{int}}) \quad (15)$$

In practice, the normalization factor  $2^{-k/2}$  (arising from the orthonormal definition  $\mathbf{H}_k = 2^{-k/2}\mathbf{H}_k^{\text{raw}}$ ) is absorbed into the floating-point quantization scales. As a result, the core computation  $(\mathbf{X}\mathbf{H})_{\text{int}} \cdot \mathbf{H} \cdot \mathbf{W}_{\text{int}}$  involves only integer matrix multiplication, enabling efficient inference on hardware accelerators.

**Convolution** For a convolutional layer, let the input activation tensor be  $\mathbf{X}_c \in \mathbb{R}^{B \times C_{\text{in}} \times h \times w}$  and the convolutional kernel be  $\mathbf{W}_c \in \mathbb{R}^{C_{\text{out}} \times C_{\text{in}} \times L \times L}$ , where  $C_{\text{in}}$  and  $C_{\text{out}}$  denote the input and output channel dimensions, respectively, and  $h \times w$  and  $L \times L$  are the spatial resolutions of the activations and the kernel.

To apply the Hadamard transformation on convolution, we first reshape  $\mathbf{X}_c$  into a 2D matrix  $\tilde{\mathbf{X}}_c \in \mathbb{R}^{(B \cdot C_{\text{in}} \cdot h) \times w}$  by merging the batch, input-channel, and height dimensions. We then compute the transformed activations as the matrix

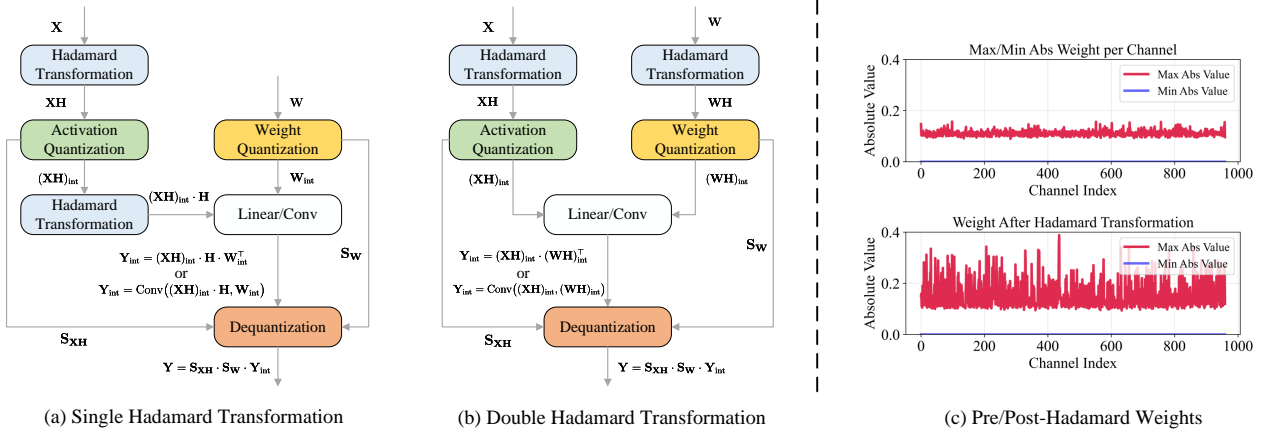


Figure 3. Schematic diagrams of Single Hadamard Transformation (a) and Double Hadamard Transformation (b). Subfigure (c) illustrates the distribution of actual matrix values, highlighting the amplified outliers following Hadamard transformation of the weights from the output\_blocks[0][1].transformer\_blocks[0].ff.net[0].proj layer on the LDM-4 model in experiments.

product  $(\tilde{\mathbf{X}}_c \mathbf{H}_c)$ , where  $\mathbf{H}_c \in \mathbb{R}^{w \times w}$  is a block-diagonal Hadamard matrix. This design ensures that the Hadamard transformation operates only along the last (width) dimension and that  $\mathbf{H}_c$  is square—allowing compatibility with standardized Hadamard orders.

Due to the orthogonality of  $\mathbf{H}_c$  ( $\mathbf{H}_c^\top = \mathbf{H}_c^{-1} = \mathbf{H}_c$ ), the original activations can be recovered from the quantized transformed representation via inverse transformation and dequantization. Specifically, let  $(\tilde{\mathbf{X}}_c \mathbf{H}_c)_{int}$  denote the integer-valued quantized form of the product  $\tilde{\mathbf{X}}_c \mathbf{H}_c$ , and let  $\mathbf{S}_{\tilde{\mathbf{X}}_c \mathbf{H}_c}$  be its associated floating-point quantization scale. The dequantized result is:

$$\hat{\mathbf{X}}_c = \mathbf{S}_{\tilde{\mathbf{X}}_c \mathbf{H}_c} \cdot (\tilde{\mathbf{X}}_c \mathbf{H}_c)_{int} \cdot \mathbf{H}_c \quad (16)$$

Consequently, the convolution operation can be rewritten using the identity  $\mathbf{H}_c \mathbf{H}_c^\top = \mathbf{I}$  as:

$$\mathbf{Y} = \text{Conv}(\mathbf{X}_c, \mathbf{W}_c) = \text{Conv}((\tilde{\mathbf{X}}_c \mathbf{H}_c) \cdot \mathbf{H}_c, \mathbf{W}_c) \quad (17)$$

$$\mathbf{Y} \approx \mathbf{S}_{\tilde{\mathbf{X}}_c \mathbf{H}_c} \mathbf{S}_{\mathbf{W}_c} \cdot \text{Conv}((\tilde{\mathbf{X}}_c \mathbf{H}_c)_{int} \cdot \mathbf{H}_c, (\mathbf{W}_c)_{int}) \quad (18)$$

Similarly, in practical implementation, the normalization factor of the Hadamard matrix  $2^{-k/2}$  can be merged with the preceding floating-point quantization factors, so that the convolution operation is performed only on integer matrices.

**Single Hadamard Transformation** For any standard basis vector  $\mathbf{e}_i \in \mathbb{R}^{2^k}$  (i.e., a vector with a single entry equal to 1 and all others 0), the product  $\mathbf{e}_i^\top \mathbf{H}_k$  yields a constant vector:

$$\mathbf{e}_i^\top \mathbf{H}_k = 2^{-k/2} \cdot \mathbf{1}_{2^k} \quad (19)$$

where  $\mathbf{1}_{2^k} = (1, 1, \dots, 1)^\top \in \mathbb{R}^{2^k}$ . This property implies that when the input vector contains a dominant outlier—i.e., one coordinate significantly larger than the rest—the Hadamard transformation effectively maps it to a uniform (flat) vector. Such a structure is highly favorable for quantization, as the resulting equal-valued entries simplify the quantization process and improve its efficiency. However, similarly, applying a Hadamard transformation to a vector with uniformly distributed elements will increase the outliers in its distribution. For example, a vector with all elements equal to 1 (i.e.  $\mathbf{1}_{2^k}$ ) yields  $(2^{k/2}, 0, 0, \dots, 0)$  after transformation, which significantly amplifies the outliers in the resulting vector.

$$\mathbf{1}_{2^k} \mathbf{H}_k = 2^{k/2} \mathbf{e}_1^\top \quad (20)$$

While previous research has employed Hadamard transformation to enhance model performance, the Hadamard transformation utilized in HQ-DM differs significantly from conventional approaches: we designate our method as the Single Hadamard Transformation, in contrast to the conventional Double Hadamard Transformation (see Figure 3 (a) (b)). The primary distinction lies in the computational methodology. Conventional Double Hadamard Transformation attempts to insert Hadamard transformation between the operations of  $\mathbf{X}$  and  $\mathbf{W}$ , enabling online quantization of  $\mathbf{XH}$  while performing  $\mathbf{H}^\top \mathbf{W}$  quantization offline. This approach introduces two critical limitations: 1) inadequate support for convolution operations in diffusion models (due to the non-applicability of matrix multiplication distributive property to convolutions, especially for multi strides), and 2) increased outliers in the weight matrix  $\mathbf{W}$  when computing  $\mathbf{H}^\top \mathbf{W}$  with originally low-outlier  $\mathbf{W}$  matrices, consequently amplifying quantization errors and degrading

model performance (see Figure 3 (c)). Our proposed Single Hadamard Transformation not only minimizes outlier introduction in weight matrices but also provides excellent convolution support. More importantly, by extracting the floating-point factor  $2^{-k/2}$ , the  $\mathbf{H}_k^{\text{raw}}$  matrix becomes a sparse integer matrix, enabling efficient hardware implementation of intermediate results through integer matrix multiplication.

**Hardware-Friendly Scheme** Single Hadamard Transformation possesses the following characteristics: its transformation of activation matrices renders activations more amenable to quantization, thereby achieving high efficiency for low-bit integer arithmetic. In contrast to several existing approaches that employ asymmetric quantization for activations (like EfficientDM), HQ-DM adopts symmetric quantization for activations, ensuring compatibility with hardware acceleration for integer matrix multiplication. While this approach effectively reduces the available quantization bits by one compared to asymmetric quantization in extreme cases, experimental results still demonstrate the substantial advantages of HQ-DM. Furthermore, as previously discussed, the Single Hadamard Transformation enables direct execution of integer matrix multiplication and convolution operations without requiring subsequent dequantization, establishing it as a hardware-friendly scheme.

## 5. Experiments

### 5.1. Experiments Settings

We conduct experiments on conditional generation using ImageNet 256×256 [9] and unconditional generation on both LSUN-Bedrooms 256×256 and LSUN-Churches 256×256 [65]. For our experiments, we employ the Latent Diffusion Models (LDM) from Stable Diffusion along with the DDIM sampler [51]. Trainable parameters are optimized using the AdamW optimizer [26], with distinct initial learning rates assigned to activation quantization factors, weight quantization factors, and LoRA low-rank matrices. For evaluation, we utilize generated sample batches of 50,000 images from each model and compute metrics against reference batches. The primary evaluation metrics include Inception Score (IS) [46], Fréchet Inception Distance (FID) [20], sFID [37], Precision and Recall. We compare our results with several prominent works in the field, including Q-Diffusion [30], PTQ-D [18], QuEST [57], TFMQ-DM [23], and EfficientDM [19]. Our experiments cover multiple quantization bit configurations, where  $WxAy$  denotes x-bit weight quantization and y-bit activation quantization respectively. More details can be found in Appendix.

### 5.2. Experiment Results

Method	Bit (W/A)	IS $\uparrow$	FID $\downarrow$	sFID $\downarrow$	Precision $\uparrow$ (%)
FP	32/32	365.35	11.22	7.78	93.68
Q-Diffusion	8/8	350.93	10.60	9.29	92.46
PTQD	8/8	359.78	10.05	9.01	93.00
EfficientDM	8/8	363.71	11.02	7.65	93.80
<b>HQ-DM</b>	<b>8/8</b>	<b>363.22</b>	<b>11.01</b>	<b>7.76</b>	<b>93.46</b>
Q-Diffusion	8/4	–	–	–	–
PTQD	8/4	–	–	–	–
EfficientDM	8/4	252.00	<b>6.75</b>	<b>8.48</b>	84.90
<b>HQ-DM</b>	<b>8/4</b>	<b>292.76</b>	7.68	9.93	<b>88.68</b>
Q-Diffusion	4/8	336.80	9.29	9.29	91.06
PTQD	4/8	344.72	<b>8.74</b>	7.98	91.69
EfficientDM	4/8	<b>351.97</b>	9.96	<b>7.80</b>	92.48
<b>HQ-DM</b>	<b>4/8</b>	350.22	9.85	8.37	<b>92.63</b>
PTQD	4/4	–	–	–	–
QuEST	4/4	202.45	<b>5.98</b>	–	–
EfficientDM	4/4	220.20	6.63	9.80	80.97
<b>HQ-DM</b>	<b>4/4</b>	<b>248.30</b>	6.58	<b>9.60</b>	<b>84.44</b>
PTQD	4/3	–	–	–	–
EfficientDM	4/3	8.74	99.78	65.79	27.48
<b>HQ-DM</b>	<b>4/3</b>	<b>49.62</b>	<b>33.47</b>	<b>12.09</b>	<b>54.87</b>

Table 1. Performance comparisons of fully-quantized LDM-4 models on ImageNet 256×256 dataset. The sampling process employs 20 denoising steps. We evaluate IS (higher is better), FID (lower is better), sFID (lower is better), Precision (higher is better) on these quantized models.

**Evaluation of conditional generation** We evaluate the performance of HQ-DM on ImageNet 256×256 using LDM-4. The results in Table 1 demonstrate that HQ-DM outperforms existing methods across these bit configurations, with this advantage becoming increasingly pronounced at lower activation quantization bit-widths. For the W4A4 configuration, HQ-DM surpasses the current SOTA method EfficientDM by 12.76% in Inception Score. Compared to EfficientDM, HQ-DM achieves performance improvements exceeding 100% across all four metrics under the W4A3 configuration, with approximately 99.7% enhancement in precision, thereby highlighting HQ-DM’s potential for ultra-low-bit quantization.

**Evaluation of unconditional generation** Following conventional practice, we employ the LDM-4 model for unconditional image generation on LSUN-Bedrooms 256×256, and the LDM-8 model for unconditional generation on LSUN-Churches 256×256. On LSUN-Bedrooms, HQ-DM surpasses existing quantization schemes across multiple bit configurations, achieving FID reductions of 5.56, 3.66, 3.49 and 5.98 for W8A4, W4A4, W3A4, and W4A3 settings, respectively. It is noteworthy that since HQ-DM exclusively processes activations, the accuracy of the quantized model depends on weight stability. In other words, the closer

Method	Bit (W/A)	FID ↓	sFID ↓	Precision ↑ (%)	Recall ↑ (%)
FP	32/32	7.56	14.06	51.95	41.18
TFMQ-DM	8/4	—	—	—	—
EfficientDM	8/4	17.91	19.44	40.40	<b>37.86</b>
<b>HQ-DM</b>	8/4	<b>12.35</b>	<b>16.27</b>	<b>47.31</b>	37.44
TFMQ-DM	4/4	—	—	—	—
EfficientDM	4/4	16.81	20.81	41.42	29.66
<b>HQ-DM</b>	4/4	<b>13.15</b>	<b>17.53</b>	<b>45.32</b>	<b>36.34</b>
TFMQ-DM	3/4	25.74	35.18	32.20	—
EfficientDM	3/4	20.92	22.78	<b>38.57</b>	29.38
<b>HQ-DM</b>	3/4	<b>19.22</b>	<b>19.29</b>	38.32	<b>31.92</b>
TFMQ-DM	2/4	<b>25.77</b>	36.74	—	—
EfficientDM	2/4	33.68	<b>27.19</b>	28.76	<b>20.34</b>
<b>HQ-DM</b>	2/4	28.50	30.17	<b>32.64</b>	18.76
EfficientDM	4/3	26.80	24.01	33.43	29.02
<b>HQ-DM</b>	4/3	<b>21.88</b>	<b>22.15</b>	<b>34.52</b>	<b>29.10</b>

Table 2. Performance comparisons of fully-quantized LDM-4 models on LSUN-Bedrooms 256×256 dataset. The sampling process employs 100 denoising steps. We evaluate FID (lower is better), sFID (lower is better), Precision (higher is better), and Recall (higher is better) on these quantized models.

the quantized weights remain to the original floating-point model, the lower the activation quantization loss achieved by HQ-DM. On LSUN-Churches, HQ-DM also outperforms EfficientDM at low quantization bit-widths. Compared to EfficientDM, HQ-DM reduces the FID by 3.19 under the W4A4 configuration and by 6.3 under W4A3. It is noteworthy that these improvements were achieved while employing hardware-friendly symmetric quantization, which typically incurs an adverse impact on performance. Across both LSUN datasets, we consistently observe that the performance gains from HQ-DM become increasingly pronounced as activation quantization bit-width decreases.

Method	Bit (W/A)	FID ↓	sFID ↓	Precision ↑ (%)	Recall ↑ (%)
FP	32/32	6.17	20.98	59.96	48.54
EfficientDM	4/4	12.83	30.04	52.61	33.69
<b>HQ-DM</b>	4/4	<b>9.64</b>	<b>28.46</b>	<b>57.10</b>	<b>35.91</b>
EfficientDM	4/3	20.97	36.56	46.25	26.06
<b>HQ-DM</b>	4/3	<b>14.67</b>	<b>31.94</b>	<b>53.22</b>	<b>27.08</b>

Table 3. Performance comparisons of fully-quantized LDM-8 models on LSUN-churches 256×256 dataset. The sampling process employs 100 denoising steps. We evaluate FID (lower is better), sFID (lower is better), Precision (higher is better), and Recall (higher is better) on these quantized models.

**Distillation Training Performance** Figure 4 illustrates the convergence characteristics of HQ-DM under W4A4

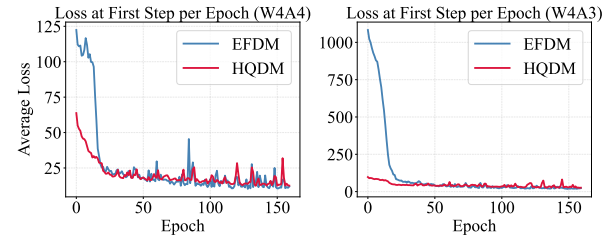


Figure 4. Loss variation versus epochs for W4A4 and W4A3 training on the ImageNet 256×256 dataset. We observe the loss change at step 0, as the first step of the training denoising process corresponds to the final step of the inference denoising output.

and W4A3 distillation training settings. The results indicate that HQ-DM achieves more stable convergence compared to EfficientDM, with accelerated convergence rates. As the activation quantization bit-width decreases, the acceleration and stability of training become increasingly pronounced.

### 5.3. Ablation Study

To investigate the impact of the order of the original Hadamard matrix on diffusion model quantization, we conducted the following ablation study: we performed W4A4 quantization on the LDM-4 model using the ImageNet 256×256 dataset, while varying the order of the original Hadamard matrix among values of 3, 4, 5, and 6. As previously discussed, higher-order Hadamard matrices exhibit stronger capability for amortizing outliers, yet they present greater challenges in matching the corresponding diagonal Hadamard matrices. We evaluated the influence of matrix order on quantized model performance across different metrics, revealing that the optimal results are achieved when the order  $k$  equals 5, corresponding to an original Hadamard matrix of size 32×32.

Table 4. Evaluation metrics for HQ-DM with different Hadamard orders ( $k$ ) of LDM-4 on ImageNet 256×256. Higher IS and Precision (%) are better (↑); lower FID and sFID are better (↓).

Order(k)	IS ↑	FID ↓	sFID ↓	Precision (%) ↑
3	<b>249.24</b>	6.70	9.77	84.17
4	245.11	6.68	10.60	83.98
5	248.30	<b>6.58</b>	<b>9.60</b>	<b>84.44</b>
6	249.04	6.73	10.38	83.99

## 6. Conclusion

We propose HQ-DM, a novel framework that enables low-bit quantization for diffusion models. To address the outlier issue in activation values during diffusion model computation, HQ-DM employs a Single Hadamard Transformation to reduce activation outliers, thereby enhancing quantized model performance. Furthermore, this hardware-friendly

framework is capable of supporting integer convolution operations without amplifying outliers in the weights during computation, thereby enhancing performance.

## 7. Additional Visualization Results

We further present the distribution of channel-wise absolute maximum values of the activation matrices, both before and after the Single Hadamard Transformation. And we further illustrate the distinction between HQ-DM and EfficientDM on the image generation task (conditional generation for ImageNet and unconditional generation for LSUN\_Bedrooms and LSUN\_Churchs). It can be observed that HQ-DM’s advantage in generating higher-quality images becomes more pronounced as the activation quantization bits are reduced.

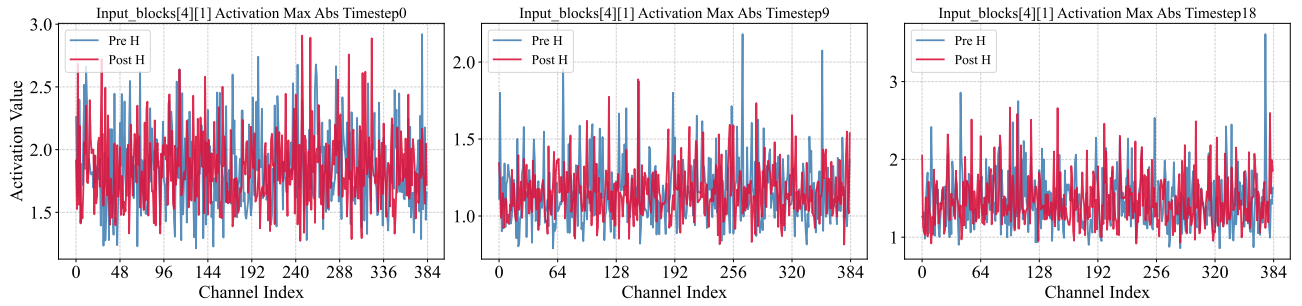


Figure 5. Channel-wise analysis of outlier distribution in activations from the input\_blocks[4] in timestep 0, 9 and 18 on LDM-4/ImageNet 256×256 dataset.

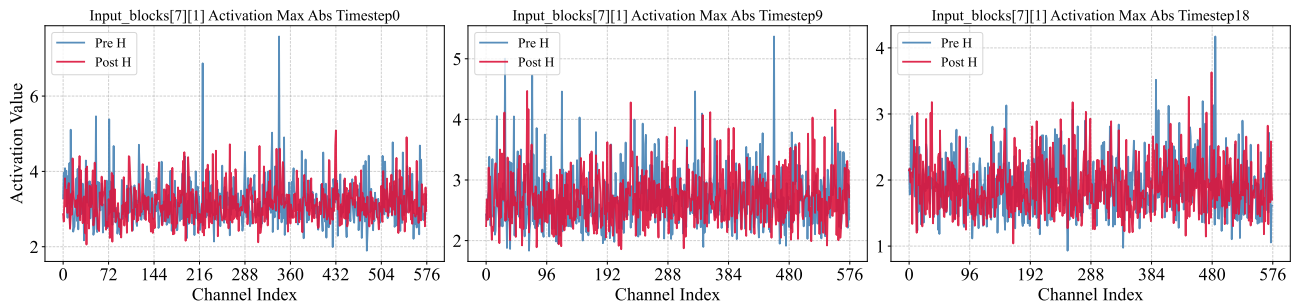


Figure 6. Channel-wise analysis of outlier distribution in activations from the input\_blocks[7] in timestep 0, 9 and 18 on LDM-4/ImageNet 256×256 dataset.

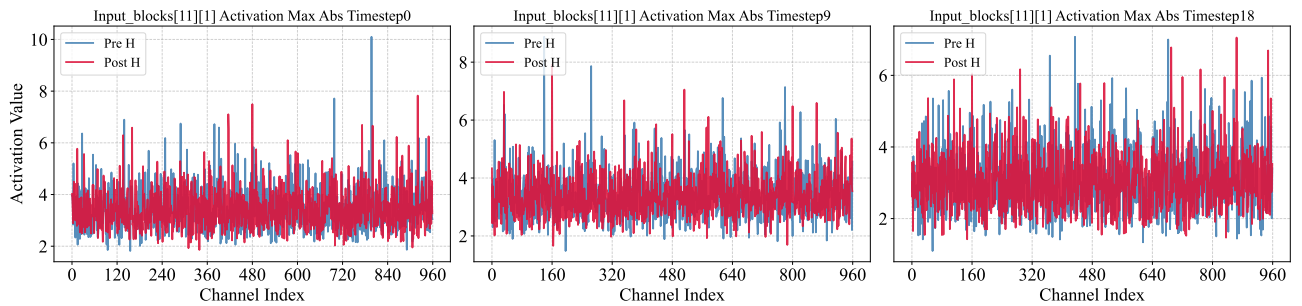


Figure 7. Channel-wise analysis of outlier distribution in activations from the input\_blocks[11] in timestep 0, 9 and 18 on LDM-4/ImageNet 256×256 dataset.

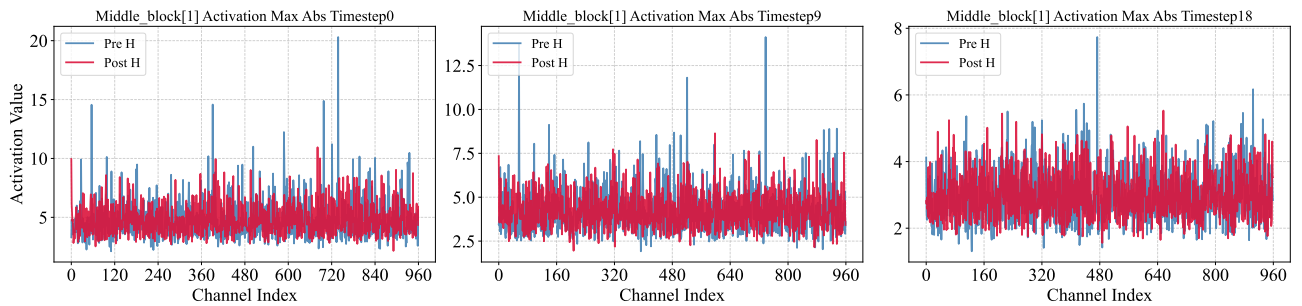


Figure 8. Channel-wise analysis of outlier distribution in activations from the middle\_block[1] in timestep 0, 9 and 18 on LDM-4/ImageNet 256×256 dataset.

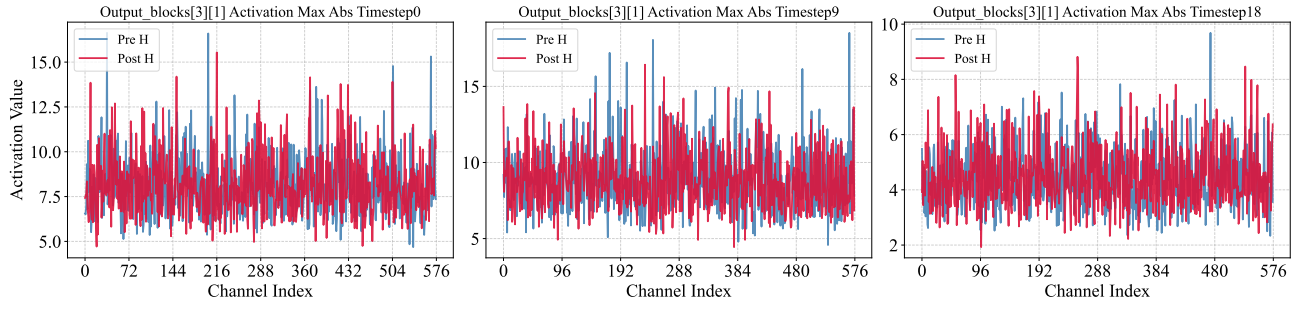


Figure 9. Channel-wise analysis of outlier distribution in activations from the output\_block[3] in timestep 0, 9 and 18 on LDM-4/ImageNet 256×256 dataset.

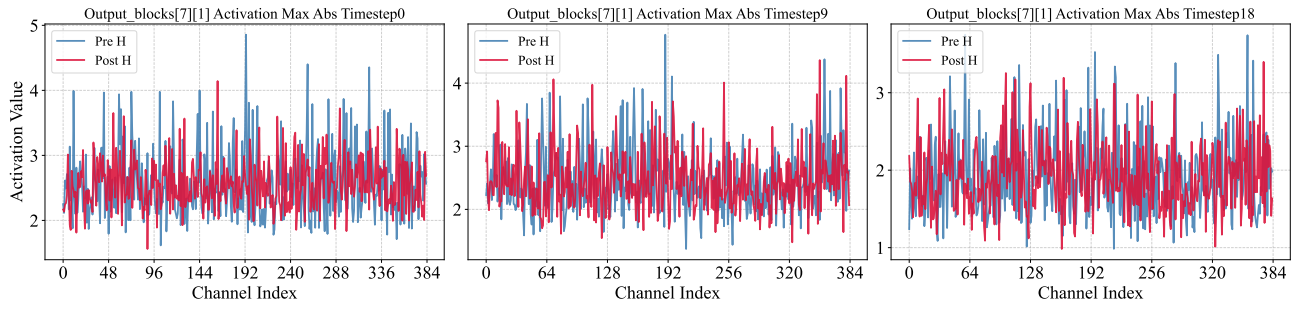


Figure 10. Channel-wise analysis of outlier distribution in activations from the output\_block[7] in timestep 0, 9 and 18 on LDM-4/ImageNet 256×256 dataset.

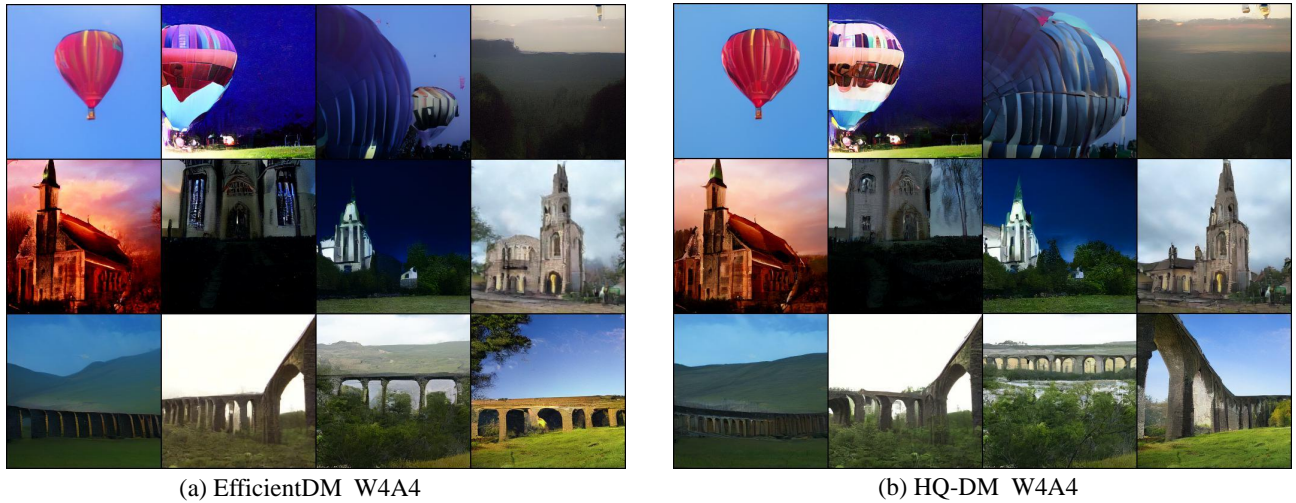


Figure 11. Comparison diagram of EfficientDM and HQ-DM generated on the ImageNet 256×256 dataset using the LDM-4 model under the W4A4 quantization configuration.



(a) FP model

(b) EfficientDM W8A3

(c) HQ-DM W8A3

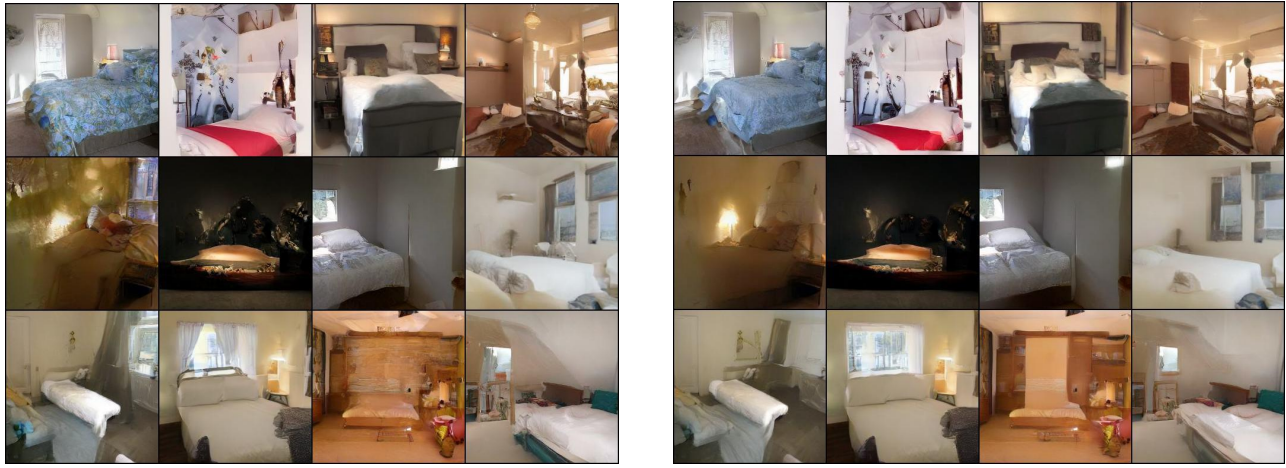
Figure 12. Comparison of FP model, EfficientDM, and HQ-DM generated on the ImageNet 256x256 dataset using the LDM-4 model under the W8A3 quantization configuration. As can be observed, HQ-DM maintains decent generation quality even with reduced activation quantization bits.



(a) EfficientDM W4A3

(b) HQ-DM W4A3

Figure 13. Comparison diagram of EfficientDM and HQ-DM generated on the LSUN-Churchs 256x256 dataset using the LDM-8 model under the W4A3 quantization configuration.



(a) EfficientDM W4A3

(b) HQ-DM W4A3

Figure 14. Comparison diagram of EfficientDM and HQ-DM generated on the LSUN-Bedrooms 256x256 dataset using the LDM-4 model under the W4A3 quantization configuration.

## References

[1] Anonymous. Effortless efficiency: Low-cost pruning of diffusion models. *arXiv preprint arXiv:2412.02852*, 2024. 1

[2] Saleh Ashkboos, Amirkeivan Mohtashami, Maximilian L Croci, Bo Li, Martin Jaggi, Dan Alistarh, Torsten Hoefler, and James Hensman. Quarot: Outlier-free 4-bit inference in rotated llms. *arXiv preprint arXiv:2404.00456*, 2024. 3

[3] Omri Avrahami, Dani Lischinski, and Ohad Fried. Blended diffusion for text-driven editing of natural images. In *IEEE/CVF Conference on Computer Vision and Pattern Recognition (CVPR)*, pages 18208–18218, 2022. 1

[4] Ron Banner, Yury Nahshan, Elad Hoffer, and Daniel Soudry. Post training 4-bit quantization of convolutional networks for rapid-deployment. In *Advances in Neural Information Processing Systems (NeurIPS) Workshops*, 2019. 3

[5] Andreas Blattmann, Robin Rombach, David Podell, and Björn Ommer. Stable video diffusion: Scaling latent video diffusion models to large datasets. In *arXiv preprint arXiv:2311.15127*, 2023. 1, 3

[6] Tim Brooks, Aleksander Holynski, and Alexei A. Efros. Instructpix2pix: Learning to follow image editing instructions. In *IEEE/CVF Conference on Computer Vision and Pattern Recognition (CVPR)*, 2023. 1

[7] Tom B. Brown, Benjamin Mann, Nick Ryder, Melanie Subbiah, Jared Kaplan, Prafulla Dhariwal, Arvind Neelakantan, et al. Language models are few-shot learners. In *Advances in Neural Information Processing Systems (NeurIPS)*, 2020. 1

[8] S. Chen et al. Exploring low-dimensional subspaces in diffusion models (loco edit). In *Advances in Neural Information Processing Systems (NeurIPS)*, 2024. 1

[9] Jia Deng, Wei Dong, Richard Socher, Li-Jia Li, Kai Li, and Li Fei-Fei. Imagenet: A large-scale hierarchical image database. In *2009 IEEE conference on computer vision and pattern recognition*, pages 248–255. Ieee, 2009. 7

[10] Tim Dettmers, Mike Lewis, Younes Belkada, and Luke Zettlemoyer. Llm.int8(): 8-bit matrix multiplication for transformers at scale. *arXiv preprint arXiv:2208.07339*, 2022. 4

[11] Abhimanyu Dubey, Xinying Song, S. Anil, et al. Gemini 1.5: Unlocking multimodal understanding across modalities. *arXiv preprint arXiv:2403.05530*, 2024. 1

[12] Steven K. Esser, Jeffrey L. McKinstry, Deepika Bablani, Rathinakumar Appuswamy, and Dharmendra S. Modha. Learned step size quantization. In *International Conference on Learning Representations (ICLR)*, 2019. 1

[13] Steven K Esser, Jeffrey L McKinstry, Deepika Bablani, Rathinakumar Appuswamy, and Dharmendra S Modha. Learned step size quantization. *arXiv preprint arXiv:1902.08153*, 2019. 5

[14] Gongfan Fang, Xinyin Ma, and Xinchao Wang. Structural pruning for diffusion models. *arXiv preprint arXiv:2305.10924*, 2023. 1

[15] Weilun Feng, Haotong Qin, Chuanguang Yang, Zhulin An, Libo Huang, Boyu Diao, Fei Wang, Renshuai Tao, Yongjun Xu, and Michele Magno. Mpq-dm: Mixed precision quantization for extremely low bit diffusion models. In *Proceedings of the AAAI Conference on Artificial Intelligence (AAAI)*, 2025. 3

[16] Weizhi Gao, Zhichao Hou, Junqi Yin, Feiyi Wang, Linyu Peng, and Xiaorui Liu. Modulated diffusion: Accelerating generative modeling with modulated quantization. In *Proceedings of the 42nd International Conference on Machine Learning (ICML)*, pages 18337–18362, 2025. 1

[17] Ian J. Goodfellow, Jean Pouget-Abadie, Mehdi Mirza, Bing Xu, David Warde-Farley, Sherjil Ozair, Aaron Courville, and Yoshua Bengio. Generative adversarial nets. In *Advances in Neural Information Processing Systems (NeurIPS)*, pages 2672–2680, 2014. 1

[18] Yefei He, Luping Liu, Jing Liu, Weijia Wu, Hong Zhou, and Bohan Zhuang. Ptqd: Accurate post-training quantization for diffusion models. In *Advances in Neural Information Processing Systems (NeurIPS)*, 2023. 3, 7

[19] Yefei He, Jing Liu, Weijia Wu, Hong Zhou, and Bohan Zhuang. Efficientdm: Efficient quantization-aware fine-tuning of low-bit diffusion models. In *International Conference on Learning Representations (ICLR)*, 2024. 3, 5, 7

[20] Martin Heusel, Hubert Ramsauer, Thomas Unterthiner, Bernhard Nessler, and Sepp Hochreiter. Gans trained by a two time-scale update rule converge to a local nash equilibrium. *Advances in neural information processing systems*, 30, 2017. 7

[21] Jonathan Ho, Ajay Jain, and Pieter Abbeel. Denoising diffusion probabilistic models. In *Advances in Neural Information Processing Systems (NeurIPS)*, pages 6840–6851, 2020. 1, 3

[22] Jonathan Ho, Tim Salimans, Ajay Jain, Ben Poole, Abhishek Kumar, Mohammad Norouzi, and William Chan. Video diffusion models. In *Advances in Neural Information Processing Systems (NeurIPS)*, 2022. 1, 3

[23] Yushi Huang, Ruihao Gong, Jing Liu, Tianlong Chen, and Xianglong Liu. Tfmq-dm: Temporal feature maintenance quantization for diffusion models. In *Proceedings of the IEEE/CVF Conference on Computer Vision and Pattern Recognition*, pages 7362–7371, 2024. 7

[24] Yushi Huang, Ruihao Gong, Jing Liu, Tianlong Chen, and Xianglong Liu. Tfmq-dm: Temporal feature maintenance quantization for diffusion models. In *IEEE/CVF Conference on Computer Vision and Pattern Recognition (CVPR)*, pages 7362–7371, 2024. 3

[25] Tero Karras, Samuli Laine, and Timo Aila. A style-based generator architecture for generative adversarial networks. In *IEEE/CVF Conference on Computer Vision and Pattern Recognition (CVPR)*, pages 4401–4410, 2019. 1

[26] Diederik P Kingma. Adam: A method for stochastic optimization. *arXiv preprint arXiv:1412.6980*, 2014. 7

[27] Raghuraman Krishnamoorthi. Quantizing deep convolutional networks for efficient inference: A whitepaper. *arXiv preprint arXiv:1806.08342*, 2018. 1

[28] Dongyeun Lee, Jiwan Hur, Hyounguk Shon, Jae Young Lee, and Junmo Kim. Dmq: Dissecting outliers of diffusion models for post-training quantization. In *Proceedings of the IEEE/CVF International Conference on Computer Vision (ICCV)*, 2025. 3

[29] B. Li et al. Few-shot temporal pruning accelerates diffusion models for text generation. In *LREC (or relevant workshop / proceedings)*, 2024. 1

[30] Xiuyu Li, Yijiang Liu, Long Lian, Huanrui Yang, Zhen Dong, Daniel Kang, Shanghang Zhang, and Kurt Keutzer. Q-diffusion: Quantizing diffusion models. In *Proceedings of the IEEE/CVF International Conference on Computer Vision (ICCV)*, pages 17535–17545, 2023. 1, 2, 3, 7

[31] Yawei Li, Shuhang Gu, Luc Van Gool, and Radu Timofte. Srdiff: Single image super-resolution with diffusion probabilistic models. In *Neurocomputing*, pages 47–59, 2022. 1, 3

[32] Haohe Liu, Yi Yuan, Xubo Liu, Mark D. Plumbley, and Wenwu Wang. Audioldm 2: Learning holistic audio generation with self-supervised pretraining. In *International Conference on Learning Representations (ICLR)*, 2024. 1

[33] Yiwei Liu, Zhizheng Wu, Ming Yang, Lei He, et al. Natural-speech 2: Latent diffusion models are natural and zero-shot speech and singing synthesizers. In *International Conference on Machine Learning (ICML)*, 2023. 1

[34] Yilun Lu, Junlin Yang, and Qifeng Chen. Dpm-solver: A fast ode solver for diffusion probabilistic model sampling in around 10 steps. In *Advances in Neural Information Processing Systems (NeurIPS)*, 2022. 1

[35] Chenlin Meng, Yutong He, Yang Song, Jiaming Song, Jiajun Wu, Jun-Yan Zhu, and Stefano Ermon. Sdedit: Image synthesis and editing with stochastic differential equations. In *International Conference on Learning Representations (ICLR)*, 2022. 1

[36] Szymon Migacz. 8-bit inference with tensorrt. In *GPU Technology Conference (GTC)*. NVIDIA, 2017. 1

[37] Charlie Nash, Jacob Menick, Sander Dieleman, and Peter W Battaglia. Generating images with sparse representations. *arXiv preprint arXiv:2103.03841*, 2021. 7

[38] Alex Nichol and Prafulla Dhariwal. Improved denoising diffusion probabilistic models. In *International Conference on Machine Learning (ICML)*, pages 8162–8171, 2021. 2, 3

[39] David Podell, Andreas Blattmann, Robin Rombach, and Björn Ommer. Sdxl: Improving latent diffusion models for high-resolution image synthesis. In *IEEE/CVF Conference on Computer Vision and Pattern Recognition (CVPR)*, 2024. 1

[40] Aditya Ramesh, Prafulla Dhariwal, Alex Nichol, Casey Chu, and Mark Chen. Hierarchical text-conditional image generation with clip latents. *arXiv preprint arXiv:2204.06125*, 2022. 3

[41] Robin Rombach, Andreas Blattmann, Dominik Lorenz, Patrick Esser, and Björn Ommer. High-resolution image synthesis with latent diffusion models. In *IEEE/CVF Conference on Computer Vision and Pattern Recognition (CVPR)*, pages 10684–10695, 2022. 1, 3

[42] Hyogon Ryu, NaHyeon Park, and Hyunjung Shim. Dgq: Distribution-aware group quantization for text-to-image diffusion models. In *International Conference on Learning Representations (ICLR)*, 2025. 1

[43] Chitwan Saharia, William Chan, Saurabh Saxena, Lala Li, Jay Whang, Emily Denton, Seyed Kamyar Seyed Ghasemipour, Burcu Karagol Ayan, Tim Salimans, Jonathan Ho, David Fleet, and Mohammad Norouzi. Photorealistic text-to-image diffusion models with deep language understanding. In *Advances in Neural Information Processing Systems (NeurIPS)*, 2022. 3

[44] Chitwan Saharia, Jonathan Ho, William Chan, Tim Salimans, David J. Fleet, and Mohammad Norouzi. Image super-resolution via iterative refinement. In *IEEE/CVF Conference on Computer Vision and Pattern Recognition (CVPR)*, pages 1957–1966, 2022. 1, 3

[45] Tim Salimans and Jonathan Ho. Progressive distillation for fast sampling of diffusion models. In *International Conference on Learning Representations (ICLR)*, 2022. 1

[46] Tim Salimans, Ian Goodfellow, Wojciech Zaremba, Vicki Cheung, Alec Radford, and Xi Chen. Improved techniques for training gans. *Advances in neural information processing systems*, 29, 2016. 7

[47] Axel Sauer, Dominik Lorenz, Andreas Blattmann, and Robin Rombach. Adversarial diffusion distillation (add). In *European Conference on Computer Vision (ECCV)*, 2024. 1

[48] Yuzhang Shang, Zhihang Yuan, Bin Xie, Bingzhe Wu, and Yan Yan. Ptq4dm: Post-training quantization on diffusion models. *arXiv preprint arXiv:2211.15736*, 2023. 3

[49] Uriel Singer, Adam Polyak, Thomas Hayes, Xi Chen, Jonathan Ho, William Chan, and Tali Dekel. Magvit v2: Simple and scalable video generation with latent diffusion. In *IEEE/CVF Conference on Computer Vision and Pattern Recognition (CVPR)*, 2024. 1, 3

[50] Hyeonjin So, Minhyuk Sung, and Jinwoo Shin. Temporal dynamic quantization for diffusion models. In *Advances in Neural Information Processing Systems (NeurIPS)*, 2024. 2

[51] Jiaming Song, Chenlin Meng, and Stefano Ermon. Denoising diffusion implicit models. In *International Conference on Learning Representations (ICLR)*, 2021. 1, 3, 7

[52] Hugo Touvron, Thibaut Lavril, Gautier Izacard, Xavier Martinet, Marie-Anne Lachaux, et al. Llama: Open and efficient foundation language models. *arXiv preprint arXiv:2302.13971*, 2023. 1

[53] Aaron van den Oord, Sander Dieleman, Heiga Zen, Karen Simonyan, Oriol Vinyals, Alex Graves, Nal Kalchbrenner, Andrew Senior, and Koray Kavukcuoglu. Wavenet: A generative model for raw audio. In *Speech Synthesis Workshop (SSW)*, 2016. 1

[54] Aäron Van Den Oord, Nal Kalchbrenner, and Koray Kavukcuoglu. Pixel recurrent neural networks. In *International conference on machine learning*, pages 1747–1756. PMLR, 2016.

[55] Ashish Vaswani, Noam Shazeer, Niki Parmar, Jakob Uszkoreit, Llion Jones, Aidan N. Gomez, Łukasz Kaiser, and Illia Polosukhin. Attention is all you need. In *Advances in Neural Information Processing Systems (NeurIPS)*, 2017. 1

[56] Changyuan Wang, Ziwei Wang, Xiuwei Xu, Yansong Tang, Jie Zhou, and Jiwen Lu. Towards accurate post-training quantization for diffusion models. In *Proceedings of the IEEE/CVF Conference on Computer Vision and Pattern Recognition (CVPR)*, pages 16026–16035, 2024. 3

[57] Haoxuan Wang, Yuzhang Shang, Zhihang Yuan, Junyi Wu, Junchi Yan, and Yan Yan. Quest: Low-bit diffusion

model quantization via efficient selective fine-tuning. *arXiv preprint arXiv:2402.03666*, 2024. 3, 7

[58] Xintao Wang, Liangbin Xie, Chao Dong, and Ying Shan. Resshift: Efficient diffusion model for image super-resolution by residual shifting. In *European Conference on Computer Vision (ECCV)*, 2024. 1, 3

[59] Xiuying Wei, Yunchen Zhang, Yuhang Li, Xiangguo Zhang, Ruihao Gong, Jinyang Guo, and Xianglong Liu. Outlier suppression+: Accurate quantization of large language models by equivalent and effective shifting and scaling. In *Proceedings of the 2023 Conference on Empirical Methods in Natural Language Processing (EMNLP)*, pages 1648–1665, 2023. 3

[60] Haocheng Xi, Changhao Li, Jianfei Chen, and Jun Zhu. Training transformers with 4-bit integers. *Advances in Neural Information Processing Systems*, 36:49146–49168, 2023. 2, 3

[61] Guangxuan Xiao, Ji Lin, Mickael Seznec, Hao Wu, Julien Demouth, and Song Han. Smoothquant: Accurate and efficient post-training quantization for large language models. In *Proceedings of the 40th International Conference on Machine Learning (ICML)*, 2023. 3

[62] Jinheng Xie, Yuexiang Li, Yawen Huang, Haozhe Liu, Wenzheng Zhang, Yefeng Zheng, and Mike Zheng Shou. Boxdiff: Text-to-image synthesis with training-free box-constrained diffusion. In *arXiv preprint arXiv:2307.10816*, 2023. 1

[63] Zhewei Yao, Reza Yazdani Aminabadi, Minjia Zhang, Xiaoxia Wu, Conglong Li, and Yuxiong He. Zeroquant: Efficient and affordable post-training quantization for large-scale transformers, 2022. 4

[64] Tianwei Yin, Michaël Gharbi, Richard Zhang, Eli Shechtman, Fredo Durand, William T. Freeman, and Taesung Park. One-step diffusion with distribution matching distillation. In *IEEE/CVF Conference on Computer Vision and Pattern Recognition (CVPR)*, 2024. 1

[65] Fisher Yu, Ari Seff, Yinda Zhang, Shuran Song, Thomas Funkhouser, and Jianxiong Xiao. Lsun: Construction of a large-scale image dataset using deep learning with humans in the loop. *arXiv preprint arXiv:1506.03365*, 2015. 7

[66] Aohan Zeng, Xiao Liu, Zhengxiao Du, Zihan Wang, Hanyu Lai, Ming Ding, Zhuoyi Yang, Yifan Xu, Wendi Zheng, Xiao Xia, et al. Gilm-130b: An open bilingual pre-trained model. *arXiv preprint arXiv:2210.02414*, 2022. 4

[67] Huijie Zhang, Jinfan Zhou, Yifu Lu, Minzhe Guo, Peng Wang, Liyue Shen, and Qing Qu. The emergence of reproducibility and consistency in diffusion models. In *Proceedings of the 41st International Conference on Machine Learning (ICML/ICML-like) / PMLR 235*, pages 60558–60590, 2024. 1

[68] Ritchie Zhao, Yuwei Hu, Jordan Dotzel, Christopher De Sa, and Zhiru Zhang. Improving neural network quantization without retraining using outlier channel splitting. In *Proceedings of the 36th International Conference on Machine Learning (ICML)*, pages 7543–7552, 2019. 3

[69] J. Zhu et al. Mole: Mixture of low-rank experts for enhancing human-centric text-to-image diffusion. In *Advances in Neural Information Processing Systems (NeurIPS)*, 2024. 1